Absorption spectra and energy levels of Gd^{3+}, Nd^{3+}, and Cr^{3+} in the garnet $Gd_3Sc_2Ga_3O_{12}$

John B. Gruber
Department of Physics, San Jose State University, San Jose, California 95192-0106

Marian E. Hills
Chemistry Division, Naval Weapons Center, China Lake, California 93555-6001

Clyde A. Morrison and Gregory A. Turner
U. S. Army Electronics Research and Development Command, Harry Diamond Laboratories, Adelphi, Maryland 20783-1197

Milan R. Kokta
Electronics Division, Materials Group, Union Carbide Corporation, Washougal, Washington 98671
(Received 29 June 1987; revised manuscript received 4 January 1988)

Absorption spectra measured between 0.3 and 6.7 μm are reported for Gd^{3+}, Nd^{3+}, and Cr^{3+} in single-crystal gadolinium scandium gallium garnet, $Gd_3Sc_2Ga_3O_{12}$, at various temperatures. Energy levels split by the crystal field are identified between 1500 and 35000 cm^{-1} for $Gd^{3+}(4f^7)$, $Nd^{3+}(4f^3)$, and $Cr^{3+}(3d^3)$. The rare-earth ions occupy sites of D_2 point-group symmetry, and chromium ions are found primarily in sites of C_{3i} point-group symmetry. A Hamiltonian consisting of Coulombic, spin-orbit, and crystal-field terms is diagonalized to obtain theoretical energy levels for each symmetry. Empirical crystal-field parameters B_{km} were determined by fitting calculated energy levels to observed levels through a variation of the B_{km}; these were compared with a lattice-sum calculation. The rms deviations between calculated and observed levels are 1.7 cm^{-1} for Nd^{3+} (45 levels), 4.0 cm^{-1} for Gd^{3+} (14 levels), and 87.7 cm^{-1} for Cr^{3+} (35 levels).

I. INTRODUCTION

The spectroscopic properties of Nd^{3+} and Cr^{3+} in gadolinium scandium gallium garnet, $Gd_3Sc_2(GaO_4)_3$ (GSGG), have received considerable attention in recent years as the search continues for more efficient and powerful solid-state lasers.[1-11] Several years ago we undertook a theoretical analysis of the crystal-field splitting of the energy levels of Nd^{3+}, Gd^{3+}, and Cr^{3+} in GSGG.[12-14] At that time only the experimental crystal-field splitting of the ^4I_J and $^4F_{3/2}$ manifolds of Nd^{3+}:GSGG had been reported.[1,15,16] Spectra of Cr^{3+}:GSGG were interpreted by Struve and Huber[17] using the cubic-energy-level scheme of Sugano and Tanabe[18,19] as an approximation. Struve and Huber concluded that spin-orbit interaction contributed to the mixing of the $^4T_2$ and ^2E energy levels.[20] However, to our knowledge, no crystal-field splitting calculations that use the correct symmetry for Nd^{3+}, Gd^{3+}, or Cr^{3+} in GSGG have been published.

We report absorption spectra obtained for Nd^{3+}, Gd^{3+}, and Cr^{3+} in GSGG crystals at various temperatures. The observed crystal-field-split (Stark) levels are compared to calculated levels which were obtained by diagonalizing a Hamiltonian consisting of Coulombic, spin-orbit, and crystal-field terms for each symmetry type. The calculations were carried out using the 11 lowest (S,L,J) states constructed from within the $4f^3$ configuration of Nd^{3+} and the 12 lowest (S,L,J) states of $Gd^{3+}(4f^7)$. We assume that Nd^{3+} substitutes for Gd^{3+} in sites of D_2 symmetry. We also assume that Cr^{3+} ions substitute for Sc^{3+} in sites of C_{3i} (S_6) symmetry. Fluorescence spectra and absorption spectra of vibronic transitions are used to assign the Stark levels of Cr^{3+}, since pure electronic electric-dipole transitions are parity forbidden between $3d^3$ states of ions residing in sites with inversion symmetry. The diagonalization of the Hamiltonian for the Cr^{3+} ion in C_{3i} symmetry with spin-orbit interaction yields energy levels different from those obtained for cubic symmetry without spin-orbit correction.

II. EXPERIMENT

The garnet GSGG is a derivative of gadolinium gallium garnet, GGG, in which gallium that is octahedrally coordinated is replaced with scandium.[21-24] While the growth behavior of both materials is similar in many ways there are several important differences. The congruent GGG composition used to grow single crystals contains approximately 1 at. wt. % Gd^{3+} in the Ga^{3+} octahedral sites. The amount is based on octahedral Ga^{3+}. The evidence for such "spillover" into a second site is based on a comparison of lattice parameters [$Gd_3Ga_2(GaO_4)_3$, $a_0=12.376$ Å, and GGG congruent composition, $a_0=12.384$ Å]. In GSGG the Gd remains in the D_2 sites.

Dopant levels of Nd^{3+} and Cr^{3+} are better controlled in GSGG than in $Y_3Al_2(AlO_4)_3$ (YAG). While the same principles govern the distribution of these ions, the distribution coefficients are much more favorable to uniform doping in the GSGG host. With distribution coefficients of 0.6 and 1.0 for Nd^{3+} and Cr^{3+}, respectively, we ob-

 ©1988 The American Physical Society

serve very small variations of Nd^{3+} concentration and uniform distribution of Cr^{3+} in single crystals of GSGG.

The starting chemicals were 99.999 percent pure. Crystal growth following the Czochralski method was carried out using an iridium crucible 3 inches in diameter and 3 inches high under an atmosphere of nitrogen containing 2% oxygen by volume to minimize the evaporation of gallium during growth. The crystal was pulled at a rate of 0.015 inch per hour and rotated during this time at 15 revolutions per minute (rpm). The crystals obtained were 1.5 inches in diameter and 6.0 inches long. Based on the distribution coefficients for the dopant concentration in the molten phase, the crystal contained approximately 1.56 at. wt. % Nd^{3+} and 1.2 at. wt. % Cr^{3+} based on Gd^{3+} and Sc^{3+}, respectively. Single crystals grew parallel to the $\langle 111 \rangle$ direction. Optical measurements were made on discs cut parallel to the $\{111\}$ planes of the crystal.

The calcium impurity concentration in the starting materials was less than 3 ppm by weight of scandium oxide. This low concentration is important with respect to the absorption spectra of Cr^{3+} ions in garnets. The presence of Ca^{2+} ions appears to change the relative intensities of the ${}^4A_2 \rightarrow {}^4T_2$ and ${}^4A_2 \rightarrow {}^4T_1$ bands as well as introduce a broad absorption feature between 1.2 and 0.9 μm. Impurities such as Ca^{2+} ions along with the oxygen vacancies in the lattice can create different local environments for the Cr^{3+} ions which result in multiple sites having different symmetries. Our crystal did not exhibit the spectra associated with such impurities. We conclude that the Cr^{3+} ions occupied Sc^{3+} sites substitutionally.

A Nicolet Model 7199 Fourier-transform infrared spectrometer (FTIR) was used to obtain spectra between 1500 and 6000 cm^{-1}. The accuracy in determining the wavelength of the absorption peaks was limited by a combination of instrument resolution employed (0.5 cm^{-1}) and observed spectral linewidths. Absorption spectra between 2.5 and 0.3 μm (4000 to 35 000 cm^{-1}) were measured using a Cary Model 17D spectrophotometer. At 0.4 μm the accuracy is better than 2 Å based on factory calibration, and the resolution is approximately 1 Å. For data recorded at the same wavelength on both instruments, agreement is within 2 cm^{-1}.

A conduction dewar filled with liquid nitrogen or liquid helium was used to obtain crystal spectra at nominally liquid-nitrogen or liquid-helium temperatures. At least 30 min were allowed for equilibration before data were obtained. Sample temperatures were not measured. However, from previous experience in taking similar spectra we estimate the crystal temperatures as 90 and 15 K, respectively.

III. OBSERVED SPECTRA

Multiphonon absorption occurs below 1700 cm^{-1}.[14–16] The infrared spectrum and energy levels of the Nd^{3+} ion appear in Figs. 1 and 2 and in Table I. Temperature-dependent spectra establish excited Stark levels of the ground-state manifold ${}^4I_{9/2}$ of Nd^{3+} as follows: 106 cm^{-1} for Z_2, 167 cm^{-1} for Z_3, and 264 cm^{-1} for Z_4. These levels are similar to those obtained from fluorescence data of Nd^{3+}:GSGG.[1]

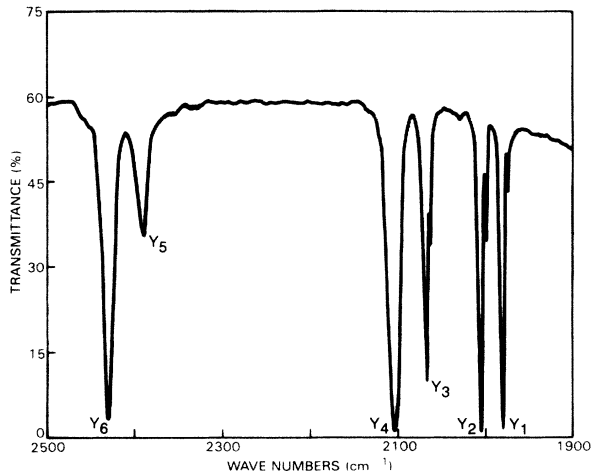

FIG. 1. Absorption spectrum of ${}^4I_{11/2}$ manifold of Nd^{3+} recorded at liquid-helium temperature with FTIR spectrometer.

In each manifold several sharp but relatively weak absorption peaks appear, usually within 3 to 8 cm^{-1} of the strong absorption peaks assigned to Nd^{3+} ions in D_2 sites of Gd^{3+}. These peaks are probably associated with Nd^{3+} ions in sites where nearby oxygen atoms are missing.[13] Consequently, the resulting Nd^{3+} ion site symmetry and crystal field are different. Nonstoichiometric loss of oxygen from the lattice during crystal growth is less of a problem for GSGG than it is for YAG. We have concentrated our analysis on the electronic transitions between all $J + \frac{1}{2}$ Stark levels in D_2 symmetry. Since each manifold contains the expected number of strong absorption peaks (usually representing more than 95 percent of the total absorption to the manifold), we assume that these peaks represent Nd^{3+} ion absorption in Gd^{3+} sites of D_2 symmetry.

The visible and near ultraviolet spectra of Nd^{3+} are given in Figs. 3–6 and in Table II. Temperature-

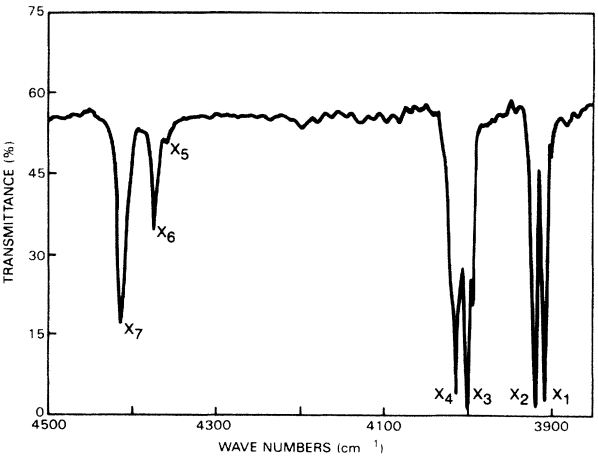

FIG. 2. Absorption spectrum of ${}^4I_{13/2}$ manifold of Nd^{3+} recorded at liquid-helium temperature with FTIR spectrometer.

dependent spectra establish the splitting of the $^4I_{9/2}$ manifold to within 1 cm^{-1} of the energy levels reported in Table I. The Z_5 energy level (763 cm^{-1}) is obtained from fluorescence data of Nd^{3+}:GSGG.[1]

Absorption by Cr^{3+} ions appears near 0.7 μm (14 200 cm^{-1}). The detailed structure of absorption bands due to vibronic transitions is obtained only at liquid-helium temperature. Electronic electric-dipole transitions are forbidden between $3d^3$ states of the same parity. Electronic magnetic-dipole transitions are allowed, and several are observed between states that are nearly pure quartet states (Table III). The vibronic spectra of Cr^{3+} ions are intense because the coupling between the lattice and the electronic states is so strong.

The R_1 and R_2 peaks of the cubic ^2E state (levels 3 and 4 in Fig. 4 and Table III) are found at 14 354 and 14 382 cm^{-1}. Peak R_2 (level 4) shows evidence of inhomogeneous line broadening (Fig. 4). These two peaks are due to electronic magnetic-dipole transitions. A band resolved into three peaks and four shoulders and nearly as intense as peaks 3 and 4 is found to the high-energy side between 14 420 and 14 470 cm^{-1}. Higher in energy is a strong, broad band due to Cr^{3+} ion absorption that begins at 0.69 μm and contains vibronic structure up to the band edge at 0.55 μm. Superimposed on this band is absorption due to Nd^{3+}. A second strong, broad band begins at 0.50 μm and extends to 0.45 μm. This band also contains Cr^{3+} vibronic structure and electronic spectra of Nd^{3+}.

To distinguish between the vibronic spectrum of Cr^{3+} and the electronic spectrum of Nd^{3+}, we analyzed the spectra of Cr^{3+}:GSGG separately and found it to be consistent with the spectrum of Cr^{3+} in the codoped crystal. Figure 7 presents the absorption spectrum of Cr^{3+}:GSGG. At liquid-helium temperature, the temperature-dependent vibronic spectra of Cr^{3+} largely disappear so that if a zero-phonon electronic transition were allowed, it would be found near the low-energy side of the observed vibronic spectra of the excited electronic state. The fluorescence spectrum observed at liquid-helium temperature also helps to establish the location of the excited Stark level. Several authors describe the use of fluorescence data to establish excited Stark levels.[15–17] Some years ago Satten and his co-workers analyzed the vibronic spectra of ions in sites of inversion symmetry.[24]

TABLE I. Infrared energy levels; Nd^{3+}. Spectra recorded using the FTIR spectrometer at room temperature (RT), liquid-nitrogen (LN) temperature, and liquid-helium (LHe) temperature. $^4I_{15/2}$ manifold recorded on spectrophotometer. Where data overlap, energy levels agree within 1 cm^{-1}.

$^{2S+1}L_J$	Label	E (cm^{-1}) RT	E (cm^{-1}) LN	E (cm^{-1}) LHe	E (cm^{-1})[a] Calc.	ΔE (cm^{-1})[b]
$^4I_{9/2}$[c]	Z_1	0	0	0	−1	−1
323[d]	Z_2	105	106	106	106	0
	Z_3	167	167	168	168	0
	Z_4	263	264		265	
	Z_5		763[c]		762	
$^4I_{11/2}$	Y_1	1979	1979	1980	1981	1
2182[d]	Y_2	2002	2003	2004	2005	1
	Y_3	2067	2067	2068	2066	−2
	Y_4	2102	2102	2103	2103	0
	Y_5	2383	2389	2391	2392	1
	Y_6	2423	2430	2432	2432	0
$^4I_{13/2}$	X_1	3908	3908	3908	3908	0
4151[d]	X_2	3917	3917	3917	3918	1
	X_3	4000	3999	4000	4000	0
	X_4	4013	4011	4012	4009	−3
	X_5	4352	4357	4359	4362	3
	X_6	4363	4371	4372	4371	−1
	X_7	4405	4411	4412	4412	0
$^4I_{15/2}$	W_1	5777	5777	5778	5778	0
6192[d]	W_2	5810	5813	5813	5812	−1
	W_3	5910	5912	5913	5914	1
	W_4	5947	5951	5954	5957	3
	W_5	6493	6495	6497	6496	−1
	W_6	6508	6510	6510	6510	0
	W_7	6547	6553	6557	6557	0
	W_8	6640	6642	6643	6642	−1

[a]Calculated energy levels based on parameters appearing in Table VI, column 6, $Nd^{3+}(B)$.

[b]Difference between calculated and observed levels at liquid-helium temperatures.

[c]Fluorescence spectra at LN temperature, Ref. 1, provide complete splitting of $^4I_{9/2}$ manifold as follows: $Z_1(0)$, $Z_2(107)$, $Z_3(168)$, $Z_4(263)$, $Z_5(763)$, all in cm^{-1}.

[d]Theoretical centroid in cm^{-1}.

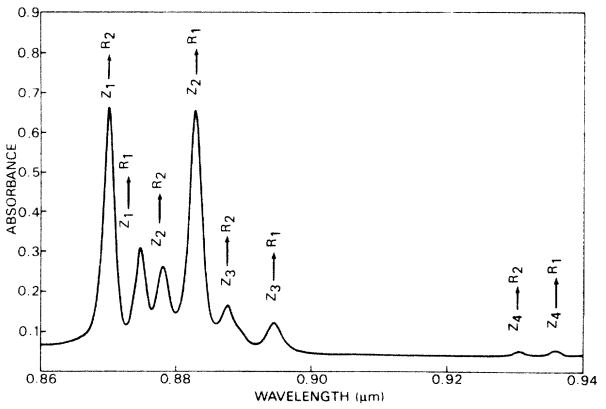

FIG. 3. Absorption spectrum of $^4F_{3/2}$ manifold of Nd^{3+} recorded at room temperature showing temperature-dependent transitions from Stark levels Z_2 (106 cm^{-1}), Z_3 (167 cm^{-1}), and Z_4 (263 cm^{-1}) of the ground-state manifold $^4I_{9/2}$.

Recently vibronic states in C_{3i} symmetry were analyzed and the Stark levels reported.[25,26] The method of analysis of vibronic spectra used here is based on the detailed descriptions reported earlier.[25,26] The observed Stark levels for Nd^{3+} are presented in Table II and those inferred from vibronic analysis for Cr^{3+} are presented in Table III. Table IV lists the energy levels of Gd^{3+}. The spectrum of Gd^{3+} appears in Fig. 8.

IV. CRYSTAL-FIELD SPLITTING CALCULATIONS: Nd^{3+} AND Gd^{3+}

Crystallographic data for the garnet GSGG are given in Table V. The crystal-field splitting of the $4f^n\,^{2S+1}L_J$ manifolds, assuming that Gd^{3+} and Nd^{3+} occupy sites of

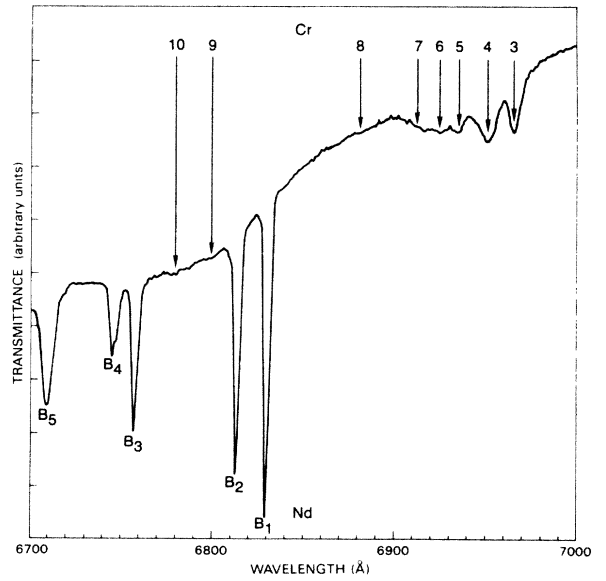

FIG. 4. Absorption spectrum of Cr^{3+} levels 3–10 and $^4F_{9/2}$ manifold (B group) of Nd^{3+} recorded at liquid-helium temperature.

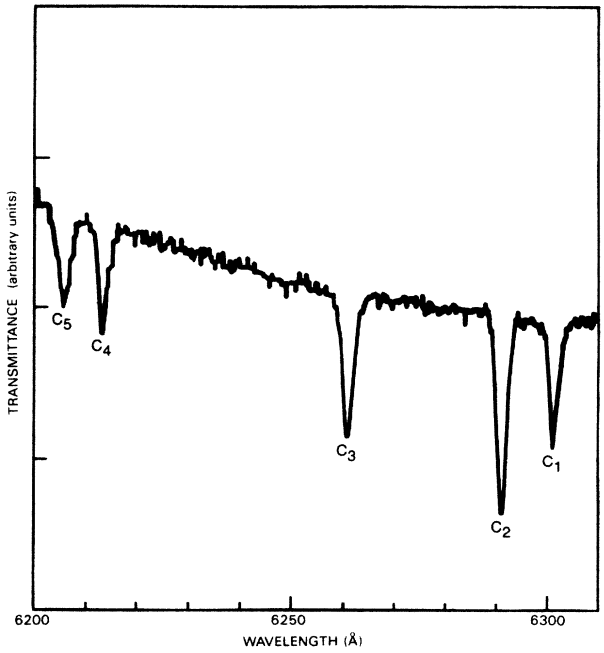

FIG. 5. Absorption spectrum of $^2H_{11/2}$ manifold of Nd^{3+} superimposed on the first strong Cr^{3+} band. Spectrum was recorded at liquid-helium temperature.

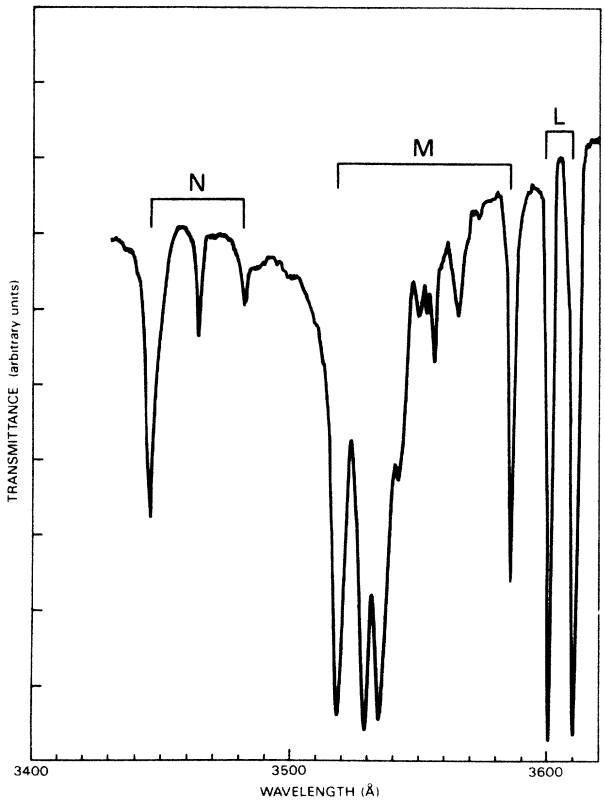

FIG. 6. Absorption spectrum of $^4D_{3/2}$ (L group), $^4D_{5/2}$ and $^2I_{11/2}$ (M group), and part of $^4D_{7/2}$ and $^2I_{13/2}$ (N group) manifolds of Nd^{3+} superimposed on the third Cr^{3+} band recorded at liquid-helium temperature.

TABLE II. Visible and ultraviolet energy levels; Nd^{3+}. Spectra recorded on spectrophotometer at room temperature (RT), liquid-nitrogen (LN) temperature, and liquid-helium (LHe) temperature.

$^{2S+1}L_J$	Label	E (cm^{-1}) RT	E (cm^{-1}) LN	E (cm^{-1}) LHe	E (cm^{-1})[a] Calc.	ΔE (cm^{-1})[b]
$^4F_{3/2}$	R_1	11 431	11 432	11 432	11 432	0
11 497[c]	R_2	11 492	11 494	11 494	11 494	0
$^4F_{5/2}$	S_1	12 350	12 352	12 354	12 348	−6
12 474[c]	S_2	12 395	12 390	12 390	12 392	2
$^2H_{9/2}$	S_3	12 395	12 404	12 405	12 405	0
12 592[c]	S_4	12 540	12 543	12 544	12 544	0
	S_5	12 580	12 584	12 586	12 590	4
	S_6	12 610	12 617	12 618	12 618	0
	S_7	12 743	12 745	12 745	12 746	1
	S_8	12 790	12 791	12 793	12 791	−2
$^4F_{7/2}$	A_1	13 372	13 374	13 374	13 375	1
13 455[c]	A_2	13 429	13 430	13 430	13 432	2
	A_3	13 550	13 553	13 555	13 556	1
$^4S_{3/2}$	A_4	13 560	13 566	13 566	13 567	1
13 547[c]	A_5	13 570	13 572	13 573	13 572	−1
	A_6	13 608	13 610	13 611	13 609	−2
$^4F_{9/2}$	B_1	14 634	14 637	14 639	14 641	2
14 724[c]	B_2	14 669	14 671	14 673	14 675	2
	B_3	14 786	14 789	14 791	14 789	−2
	B_4	14 804	14 806	14 810	14 809	−1
	B_5	14 899	14 900	14 902	14 901	−1
$^2H_{11/2}$	C_1	15 864	15 865	15 865		
	C_2	15 888	15 890	15 890		
	C_3	15 965	15 966	15 967		
	C_4	16 086	16 090	16 091		
	C_5	16 105	16 109	16 110		
$^4G_{5/2}$	D_1	16 907	16 909	16 910		
	D_2	17 000	17 005	17 008		
$^2G_{7/2}$	D_3		17 020	17 022		
	D_4	17 070	17 074	17 075		
	D_5	17 278	17 282	17 284		
	D_6		17 550	17 557		
	D_7	17 563	17 570	17 573		
$^4G_{7/2}$	E_1	18 777	18 781	18 783		
	E_2	18 864	18 864	18 864		
	E_3	18 881	18 883	18 884		
	E_4	18 997	19 001	19 004		
$^2K_{13/2}$	F_1	19 203	19 205	19 207		
	F_2	19 236	19 238	19 238		
$^2G_{9/2}$	F_3	19 330	19 334	19 335		
	F_4	19 354	19 359	19 359		
	F_5	19 410	19 411	19 412		
	F_6	19 480	19 487	19 488		
	F_7	19 518	19 520	19 521		
	F_8	19 586	19 590	19 592		
	F_9	19 615	19 619	19 620		
	F_{10}	19 670	19 672	19 672		
	F_{11}	19 820	19 824	19 824		
	F_{12}	19 890	19 895	19 895		
$^4G_{9/2}$	G_1	20 793	20 795	20 797		
	G_2	20 824	20 828	20 828		
	G_3	20 842	20 845	20 846		

TABLE II. (*Continued*).

$^{2S+1}L_J$	Label	E (cm^{-1}) RT	E (cm^{-1}) LN	E (cm^{-1}) LHe	E (cm^{-1})[a] Calc.	ΔE (cm^{-1})[b]
$^4G_{11/2}$	G_4	20 852	20 856	20 858		
	G_5	20 977	20 980	20 980		
	G_6	21 040	21 042	21 043		
	G_7	21 093	21 096	21 096		
	G_8	21 143	21 145	21 146		
	G_9	21 158	21 159	21 159		
	G_{10}	21 203	21 206	21 207		
	G_{11}	21 234	21 238	21 240		
$^2K_{15/2}$	H_1	21 609	21 610	21 611		
	H_2	21 714	21 714	21 714		
	H_3	21 740	21 740	21 742		
	H_4	21 772	21 773	21 774		
	H_5	21 778	21 780	21 783		
	H_6	21 884	21 884	21 885		
	H_7	22 004	22 005	22 006		
	H_8	22 053	22 054	22 054		
$^2P_{1/2}$	I_1	23 190	23 192	23 193		
$^2D_{5/2}$	J_1	23 723	23 723	23 724		
	J_2	23 778	23 779	23 780		
	J_3	23 832	23 840	23 843		
$^2P_{3/2}$	K_1	26 045	26 046	26 047		
	K_2		26 055	26 056		
$^4D_{3/2}$	L_1	27 685	27 689	27 689		
	L_2	27 761	27 765	27 765		
$^4D_{5/2}$	M_1	27 880	27 880	27 882		
	M_2	28 035	28 039	28 040		
$^4D_{1/2}$	M_3	28 105	28 112	28 113		
	M_4	28 145	28 150	28 159		
	M_5	28 280	28 283	28 284		
$^2I_{11/2}$	M_6	28 328	28 333	28 335		
	M_7	28 409	28 413	28 413		
	M_8	28 705	28 712	28 714		
	M_9	28 853	28 857	28 859		
	M_{10}	29 014	29 017	29 018		
$^2L_{15/2}$	N_1	29 853	29 854	29 856		
	N_2	29 963	29 960	29 958		
	N_3			29 969		
$^4D_{7/2}$	N_4	29 993	29 997	30 000		
	N_5	30 051	30 056	30 059		
	N_6		30 070	30 073		
	N_7	30 178	30 180	30 180		
	N_8	30 209	30 210	30 210		
	N_9	30 263	30 264	30 265		
	N_{10}	30 300	30 306	30 308		
	N_{11}	30 352	30 356	30 359		
$^2I_{13/2}$	N_{12}	30 428	30 430	30 431		
	N_{13}	30 453	30 453	30 454		
	N_{14}	30 506	30 509	30 510		
	N_{15}	30 532	30 536	30 540		
	N_{16}	30 625	30 627	30 630		
$^2L_{17/2}$	O_1	31 413	31 413	31 414		
	O_2	31 518	31 520	31 522		
	O_3	31 568	31 570	31 570		
	O_4	31 610	31 610	31 612		
	O_5	31 660	31 662	31 662		

TABLE II. (*Continued*).

$^{2S+1}L_J$	Label	E (cm^{-1}) RT	E (cm^{-1}) LN	E (cm^{-1}) LHe	E (cm^{-1})[a] Calc.	ΔE (cm^{-1})[b]
	O_6	31 751	31 753	31 755		
$^2H_{9/2}$	P_1	32 633	32 633	32 634		
	P_2	32 684	32 686	32 686		
	P_3	32 708	32 710	32 713		
	P_4	32 770	32 772	32 774		
	P_5	32 791	32 795	32 797		

[a]Calculated energy levels based on B_{km} parameters appearing in Table VI under column 6, $Nd^{3+}(B)$.
[b]Difference between calculated and observed levels at LHe temperature; rms deviation for 45 levels (Tables I and II) is 1.7 cm^{-1}.
[c]Theoretical centroid in cm^{-1}.

D_2 point-group symmetry, was analyzed by diagonalizing a parametrized Hamiltonian,

$$H_{D_2}=\sum_{k,m} B_{km}C_{km} , \tag{1}$$

in a free-ion wave-function basis involving the 11 lowest $4f^3\,^{2S+1}L_J$ manifolds for Nd^{3+} and the 12 lowest $4f^7\,^{2S+1}L_J$ manifolds for Gd^{3+}.[23] Free-ion wave functions and reduced matrix elements of the $U^{(k)}$ unit spherical tensors were first obtained by diagonalizing the free-ion Hamiltonian using parameters reported earlier.[27] The nine real, even-fold (even-k) parameters in the D_2 Hamiltonian were varied to obtain agreement with observed splitting. The equations given in Ref. 14 can be used to obtain the relationships between the B_{km} parameters and the $A_k^m\langle r^k\rangle$ and $\bar{B}_{km}$ parameters which are frequently reported; also given in Ref. 14 are the six possible equivalent sets of B_{km} parameters for D_2 symmetry.

An initial set of empirical B_{km} parameters for Nd^{3+} was used from an earlier report.[23] We extend that work by including data and calculations for the additional Nd^{3+} manifolds, $^4F_{5/2}$, $^2H_{9/2}$, $^4F_{7/2}$, $^4S_{3/2}$, and $^4F_{9/2}$. Table VI presents the final set of B_{km} parameters based on the experimental energy levels listed in Tables I and II. The calculated splittings are also listed in Tables I and II. An rms deviation of 1.7 cm^{-1} is obtained for 45 observed levels using the final set of empirical B_{km} parameters under column Nd(B) (Table VI).

The empirical B_{km} parameters were compared with those obtained from a lattice-sum calculation.[23] The fractional oxygen positions were taken from the isostructural material $Y_3Ga_2(GaO_4)_3$.[14] Effective charges Z_i ($q_i=eZ_i$) were chosen to be $Z_{Gd}=Z_{Sc}=3$, $Z_{Ga}=1$, $Z_O=-1.5$. The polarizibility of oxygen α_0 was taken as 0.244 $Å^3$. Table VI lists the resulting lattice sums A_{km}, which include the point-charge, point-dipole, and self-induced contributions. The parameters A_{km} are related to the B_{km} parameters through the expression

$$B_{km}=\rho_k(\mathrm{Nd})A_{km} , \tag{2}$$

where ρ_k(Nd) are radial factors given by Morrison, Karayianis, and Wortman.[28] The lattice-sum calculation predicts reasonable values for A_{km} considering our assumptions.

The set of B_{km} parameters for Gd^{3+} was obtained by using ρ_k(Gd) and the empirical A_{km} lattice parameters from Table VI. The 14 observed energy levels for Gd^{3+} are marginal for a meaningful analysis, since D_2 symmetry requires nine crystal-field parameters. The rms deviation for these levels is 4 cm^{-1}, which is within the uncertainty associated with the data recorded in the ultraviolet region.

V. CRYSTAL-FIELD SPLITTING CALCULATIONS: Cr^{3+}

A detailed analysis of the crystal-field splitting of the electronic states of Cr^{3+} in sites of C_{3i} symmetry is described here. The free-ion Hamiltonian is given by

$$H_{\mathrm{FI}}=\sum_{k=2,4} F^{(k)}\sum_{i>j}^{N} C_{kq}^*(i)C_{kq}(j) +\alpha L(L+1)+\gamma G(R_5)+\zeta_d\sum_{i=1}^{N} l_i\cdot s_i , \tag{3}$$

where $F^{(k)}$ are the Slater integrals, α and γ are parameters of the Tree's interactions, and ζ_d is the spin-orbit parameter. In Eq. (3), the Slater integrals are related to the Racah parameters by

$$F^{(2)}=7(7B+C) , \quad F^{(4)}=63C/5 , \tag{4}$$

and the C_{kq} are related to the spherical harmonics by

$$C_{kq}(i)=\sqrt{4\pi/(2k+1)}\,Y_{kq}(\theta_i,\phi_i) , \quad C_{k,-q}=(-1)^qC_{kq}^* . \tag{5}$$

The quantity $G(R_5)$ is the Casimir operator for the rotation group R_5, whose values for all the states of d^N are given by Judd.[29]

For the Cr^{3+} free ion, the parameters in Eq. (3) have the following values from Uylings, Raassen, and Wyart:[30] $F^{(2)}=74\,201$ cm^{-1}, $F^{(4)}=45\,822$ cm^{-1}, $\alpha=29.87$ cm^{-1}, and $\zeta_d=275$ cm^{-1}. We obtained the values $F^{(2)}=72\,389$ cm^{-1}, $F^{(4)}=43\,044$ cm^{-1}, $\alpha=91.75$ cm^{-1}, $\gamma=-129.6$ cm^{-1}, and $\zeta_d=277.7$ cm^{-1}, using Eq. (3) in a least-squares fit to the data reported by Sugar and Corliss.[31] Since our parameters agree well with those of Uylings and co-workers, we assume that Eq. (3) is an adequate representation of the free-ion interactions for transition metal ions in a solid. The principal difference between

our parameters and those of Uylings and co-workers is the inclusion of the Trees interaction with the parameter T and a parameter β, which multiplies the seniority operator.

The crystal-field Hamiltonian for Cr^{3+} in Sc^{3+} sites is

$$H_{CF}=B_{20}\sum_{i=1}^{N}C_{20}(i)+B_{40}\sum_{i=1}^{N}C_{40}(i)+B_{43}\sum_{i=1}^{N}[C_{4-3}(i)-C_{43}(i)]\,, \quad (6)$$

where B_{kq} are crystal-field parameters; B_{43} is chosen as real and positive with no loss in generality. In the cubic approximation, $B_{20}=0$ and $B_{43}=\sqrt{10/7}\,|B_{40}|$ in cm^{-1}. In threefold symmetry $B_{40}=-14Dq$, where we assume Dq is a positive number.

The matrix elements of the Hamiltonian given in Eqs. (3) and (6) were computed using coefficients of fractional parentage for the d^3 configuration. The notation of the free-ion levels is that given by Nielson and Koster.[32] Total angular momentum wave functions are used. The Γ_4

TABLE III. Absorption spectra of Cr^{3+} at liquid-helium temperature.

L	λ (Å)	$\Delta\lambda$[a] (Å)	I	E_{obs} (cm^{-1})	E_{calc}[b] (cm^{-1})	Representation[c] Γ_n	Free-ion state[d] (%)
1				0	−37[e]	4	100 ^4F
2					−37	6	100 ^4F
3	6965	10	0.15	14 354	14 296	6	85 ^4F+9 ^2G+3 ^2H
4	6951	10	0.19	14 382	14 328	4	94 ^4F+4 ^2G+1 ^2H
5	6933	8	0.15	14 420	14 436	4	79 ^4F+13 ^2G+4 ^2H
6	6923	10	0.14	14 440	14 480	6	87 ^4F+8 ^2G+3 ^2H
7	6909	10	0.12	14 470	14 486	4	100 ^4F
8	6879	5	0.02	14 533	14 540	4	96 ^4F+2 ^2G+1 ^2H
9	6795	10	0.04	14 714	14 831	6	45 ^2G+26 ^4F+15 ^2H
10	6776	5	0.03	14 754	14 842	4	44 ^2G+27 ^4F+16 ^2H
11	6632	8	0.03	15 074	15 176	6	39 ^2G+35 ^2H+19 ^2P
12	6535	20	0.02	15 298	15 244	4	39 ^2G+33 ^2H+19 ^2P
13	6360	500	0.43	15 719	15 421	4	38 ^2G+34 ^2H+23 ^2P
14	5043	10	0.10	19 824	19 948	4	57 ^4F+42 ^4P
15	4993	14	0.15	20 014	19 964	6	57 ^4F+43 ^4P
16	4800	20	0.18	20 700	20 830	4	50 ^4F+48 ^4P+1 ^2H
17	4806	100	0.45	20 800	20 861	6	50 ^4P+49 ^4F
18	4783	sh[f]		20 900	20 881	4	50 ^4P+49 ^4F
19	4772		0.50	20 950	20 901	4	51 ^4P+49 ^4F
20	4650	sh[f]		21 500	21 532	4	33 ^2H+25 $^2D1$+19 $^2D2$
21	4540	100	0.45	22 020	22 014	6	40 ^2H+24 $^2D1$+17 $^2D2$
22	4524	sh[f]	0.49	22 100	22 063	4	39 ^2H+24 $^2D1$+17 $^2D2$
23	3665	10	0.01	27 277	27 185	4	100 ^2G
24	3438	5	0.02	29 078	29 020	4	55 ^2G+39 ^2H+3 $^2D2$
25	3431	5	0.01	29 138	29 083	6	57 ^2G+37 ^2H+3 $^2D2$
26	3425	5	0.03	29 189	29 120	4	53 ^2G+43 ^2H+3 $^2D2$
27	3408	10	0.06	29 334	29 477	4	51 ^2H+29 ^2G+18 ^2P
28	3395	7	0.02	29 447	29 592	4	51 ^2H+28 ^2G+20 ^2P
29					29 602	6	50 ^2H+27 ^2G+21 ^2P
30					31 258	4	47 ^2H+41 $^2D2$+8 $^2D1$
31	3198	10	0.01	31 261	31 259	6	48 ^2H+42 $^2D2$+8 $^2D1$
32	3119	5	0.04	32 052	32 068	4	50 ^4P+49 ^4F
33	3116		0.04	32 082	32 087	6	49 ^4F+49 ^4P+1 ^2H
34	3105	3	0.02	32 200	32 099	4	49 ^4F+48 ^4P+2 ^2H
35	3100	10	0.07	32 249	32 107	4	50 ^4F+48 ^4P+1 ^2H
36	3085	10	0.09	32 406	32 443	4	57 ^4P+43 ^4F
37	3081		0.03	32 440	32 444	6	56 ^4P+42 ^4F+1 ^2H

[a]Bandwidth: full width at half maximum.

[b]The parameters used in the calculation are $F^{(2)}=54\,320$ cm^{-1}, $F^{(4)}=43\,094$ cm^{-1}, $\alpha=2.88$ cm^{-1}, $\gamma=-63.28$ cm^{-1}, $\zeta_d=169.64$ cm^{-1}, $B_{20}=1072$ cm^{-1}, $B_{40}=-22\,251$ cm^{-1}, and $B_{43}=23\,443$, with an rms of 87.7 cm^{-1}. ($B=620$, $C=3420$, $Dq=1450$, $v=-377.5$, $v'=512.5$.)

[c]The irreducible representations are $4=\Gamma_4+\Gamma_5$ and $6=\Gamma_6$ (doublet) for the group C_3 or C_{3i} (all Γ_i and Γ_i^+). The notation is from Koster *et al.* (Ref. 33).

[d]Only states of 1% or greater are listed.

[e]The splitting of the ground state is 0.235 cm^{-1} with small amounts of the ^4P and ^2G mixed in.

[f]Shoulder of a band.

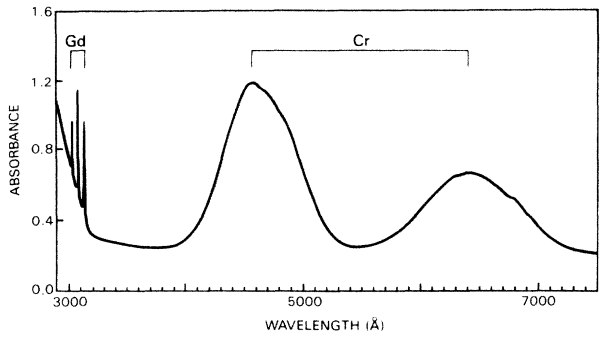

FIG. 7. Absorption spectrum of Cr^{3+}:GSGG between 3000 and 8000 Å recorded at room temperature with a Cary Model 17D spectrophotometer.

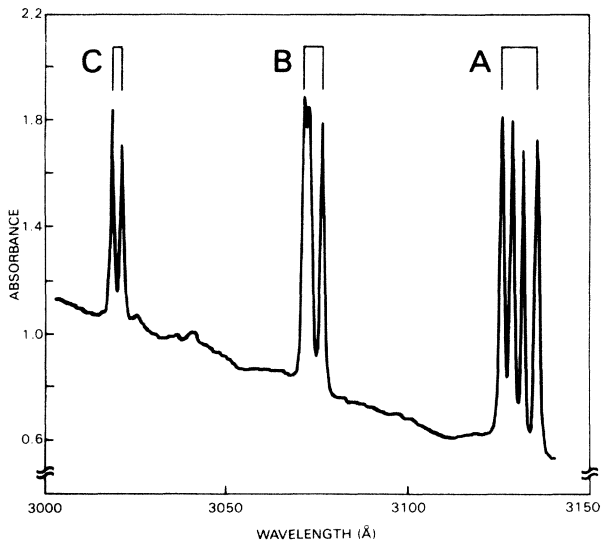

FIG. 8. Absorption spectrum of $^6P_{7/2}$ (A group), $^6P_{5/2}$ (B group), and $^6P_{3/2}$ (C group) manifolds of Gd^{3+} recorded at room temperature.

matrix elements[33] for C_3 symmetry are obtained by choosing the projection $M_J=\frac{1}{2}+3q$ with q any integer and with $|M_J|<J$. For the Γ_6 irreducible representation, we use $M_J=\frac{3}{2}+3q$, where q is any integer and $|M_J|<J$. Identical energies are calculated whether we use either $[|JM_J\rangle+(-1)^{J-M_J}|J-M_J\rangle]/\sqrt{2}$ or $[|JM_J\rangle-(-1)^{J-M_J}|J-M_J\rangle]/\sqrt{2}$ as the basis. The Hamiltonian matrices for Γ_4 and Γ_5 are 39×39 and 21×21 for Γ_6. *A priori* assumptions are not made about the relative magnitudes of the various terms in the Hamiltonian. This choice of basis, while not appropriate for cubic symmetry, avoids tedious perturbation calculations for lower symmetries.

To determine approximate atomic parameters, we began by assuming cubic symmetry. From observed spectra, we estimated the position of the experimental barycenters as $E(^4A_2)=0$ cm^{-1}, $E(^2E)=14\,368$ cm^{-1}, $E(^2T_1)=14\,436$ cm^{-1}, $E(^4T_2)=14\,793$ cm^{-1}, $E(^4T_1)=20\,330$ cm^{-1}, and $E(^4T_1)=32\,251$ cm^{-1}. In making these selections, we used a Tanabe plot[34] with $Dq=1479.3$ cm^{-1}. This value of Dq gave $B_{40}=-20\,710$ cm^{-1} and $B_{43}=24\,753$ cm^{-1}. For free-ion parameters, we started with those of Cr^{3+} in $Y_3Al_2(AlO_4)_3$ (YAG),[35] which are $F^{(2)}=55\,800$ cm^{-1}, $F^{(4)}=36\,800$ cm^{-1}, and

TABLE IV. Ultraviolet energy levels; Gd^{3+}. Spectra recorded on spectrophotometer at room temperature (RT), liquid-nitrogen (LN) temperature, and liquid-helium (LHe) temperature.

$^{2S+1}L_J$	Label	E (cm^{-1}) RT	E (cm^{-1}) LN	E (cm^{-1}) LHe	E (cm^{-1})[a] calc.	ΔE (cm^{-1})[b]
$^8S_{7/2}$	Z_1	0	0	0	0.0	0
0.4[c]	Z_2				0.3	
	Z_3				0.5	
	Z_4				0.6	
$^6P_{7/2}$	A_1	31 889	31 890	31 891	31 896	5
31 980[c]	A_2	31 926	31 927	31 927	31 922	−5
	A_3	31 958	31 960	31 961	31 966	5
	A_4	31 988	31 990	31 991	31 989	−2
$^6P_{5/2}$	B_1	32 499	32 501	32 503	32 506	3
32 573[c]	B_2	32 536	32 534	32 532	32 528	−4
	B_3	32 548	32 549	32 551	32 556	5
$^6P_{3/2}$	C_1	33 090	33 092	33 093	33 093	0
33 156[c]	C_2	33 118	33 119	33 120	33 119	−1
$^6I_{7/2}$	D_1			35 860	35 857	−3
35 879[c]	D_2			35 892	35 889	−3
	D_3			35 900	35 901	1
	D_4			35 910	35 915	5

[a]Calculated energy levels based on B_{km} parameters appearing in Table VI.
[b]Difference between calculated and observed levels at LHe temperature; rms deviation for 14 levels is 4 cm^{-1}.
[c]Theoretical centroid in cm^{-1}.

TABLE V. Crystallographic and x-ray data of $Gd_3Sc_2(GaO_4)_3$. Cubic $Ia3d$, $Z=8$. Lattice constant is $a=12.5668$ Å from Brandle and Barns (Ref. 38) and the fractional positions for the oxygen ions are for $Y_3Ga_2(GaO_4)_3$ from Euler and Bruce (Ref. 39).

Ion	Site	Symmetry	x	y	z
Gd	24c	D_2	0	$\frac{1}{4}$	$\frac{1}{8}$
Sc	16a	C_{3i}	0	0	0
Ga	24d	S_4	0	$\frac{1}{4}$	$\frac{3}{8}$
O	96h	C_1	−0.0272	0.0558	0.1501

$\alpha=\gamma=\zeta_d=0$. With these parameters as starting values, a least-squares fit to the experimental barycenters was performed. The resulting parameters obtained were $F^{(2)}=50\,200$ cm^{-1}, $F^{(4)}=40\,821$ cm^{-1}, $\alpha=35.09$ cm^{-1} ($\gamma=\zeta=B_{20}=0$ cm^{-1} not varied), $B_{40}=-20\,797$ cm^{-1}, and $B_{43}=24\,857.71$ cm^{-1}. A similar fit to the limited data of Struve and Huber[17] gave $F^{(2)}=53\,961$ cm^{-1}, $F^{(4)}=40\,782$ cm^{-1}, $B_{40}=-21\,882$ cm^{-1}, and $B_{43}=26\,154$ cm^{-1} ($\alpha=\gamma=\zeta_d=B_{20}=0$).

Proceeding now with the correct symmetry (C_{3i}) and the data given in Table V, we computed the point-charge lattice-sum parameters A_{nm},[23] which are $A_{20}=812$ cm^{-1}/Å^2, $A_{40}=-11\,413$ cm^{-1}/Å^4, and $A_{43}=13\,327$ cm^{-1}/Å^4. We used the rotational invariants[36]

$$S_n(B)=\left[B_{n0}^2+2\sum_{m>0}^{n}B_{nm}^{*}B_{nm}\right]^{1/2} \tag{7}$$

which for C_{3i} symmetry gives

$$S_4(B)=(B_{40}^2+2B_{43}^2)^{1/2} . \tag{8}$$

If we assume that the theoretical B_{nm} are given by $B_{nm}=\rho_n A_{nm}$, then $\rho_4=S_4(B)/S_4(A)$. From Eqs. (7) and (8) above we have

$$\rho_4=1.8537\ \text{Å}^4 . \tag{9}$$

If we assume further that $\rho_n=\langle r^n\rangle_{\rm HF}/\tau^n$ (with $\langle r^n\rangle_{\rm HF}$ given by a Hartree-Fock calculation and τ^n a radial expansion parameter), then

$$\rho_2=\langle r^2\rangle_{\rm HF}(\rho_4/\langle r^4\rangle_{\rm HF})^{1/2} . \tag{10}$$

From Fraga, Saxena, and Karwowski[37] we obtain values of $\langle r^2\rangle_{\rm HF}=0.4018$ Å^2 and $\langle r^4\rangle_{\rm HF}=0.3344$ Å^4 which gives $\rho_2=0.9460$ Å^2. Using ρ_2, ρ_4, and $B_{nm}^t=\rho_n A_{nm}$ we obtain

$$\begin{aligned} B_{20}^t&=786\ \text{cm}^{-1} ,\\ B_{40}^t&=-21\,156\ \text{cm}^{-1} ,\\ B_{43}^t&=24\,704\ \text{cm}^{-1} . \end{aligned} \tag{11}$$

The crystal-field parameters given in Eq. (11) were used along with the free-ion parameters obtained from the initial fitting (including $\zeta_d=200$ cm^{-1}) as starting values in a least-squares fit to all electronic energy levels established from the analysis of the vibronic spectra. A total of 35 levels of Cr^{3+} were involved in the final fit. The resulting parameters obtained were $F^{(2)}=54\,320$ cm^{-1}, $F^{(4)}=43\,094$ cm^{-1}, $\alpha=2.88$ cm^{-1}, $\gamma=-63.28$ cm^{-1}, $\zeta_d=169.64$ cm^{-1}, $B_{20}=1072$ cm^{-1}, $B_{40}=-22\,251$ cm^{-1}, and $B_{43}=23\,443$ cm^{-1}. The rms deviation is 87.7 cm^{-1}.

Table III gives the resulting energy levels, along with the percentage of the free-ion composition of each state (only values greater than 1% are given). The number of levels of the free-ion composition is limited to 3; the labels are in the convention of Nielson and Koster.[32] Because of the spin-orbit coupling and the twofold crystal field (B_{20}), the ^2E cubic level becomes predominantly ^4F, and the entire region from 14 300–15 000 cm^{-1} is so mixed that a cubic interpretation is impossible.

TABLE VI. Crystalline electric field (CEF) parameters for Nd^{3+} and Gd^{3+}.

A_{km}	A_{km}(calc.)[a] (cm^{-1}/Å)^n	A_{km}(phenomen.)[b] Nd^{3+} (cm^{-1}/Å)^n	B_{km}	$Nd^{3+}(A)$[c] (cm^{-1})	$Nd^{3+}(B)$[d] (cm^{-1})	Gd^{3+}[e] (cm^{-1})
A_{20}	3572	2544	B_{20}	434	416	154
A_{22}	1010	529	B_{22}	90	76	308
A_{40}	−8.19	−115	B_{40}	−67	−53	18
A_{42}	−3990	−3148	B_{42}	−1818	−1774	−1418
A_{44}	−2141	−1595	B_{44}	−921	−980	−699
A_{60}	−981	−934	B_{60}	−1485	−1516	−1043
A_{62}	−350	−427	B_{62}	−679	−671	−515
A_{64}	504	485	B_{64}	771	777	514
A_{66}	−337	−416	B_{66}	−661	−641	−693

[a]Table II, Ref. 23.
[b]Values of parameters A_{km} calculated from phenomenological B_{km} parameters; Ref. 23 from an analysis of fluorescence data for ^4I_J and $^4F_{3/2}$ manifolds reported in Ref. 1.
[c]Initial set of B_{km} parameters; Ref. 23.
[d]Final set of B_{km} parameters for Nd^{3+}; 45 levels; rms deviation 1.7 cm^{-1}.
[e]B_{km} parameters for Gd^{3+}; 14 levels; rms deviation 4 cm^{-1}.

VI. CONCLUSIONS

From temperature-dependent absorption spectra of Nd^{3+}:GSGG,[1] Cr^{3+}:GSGG,[17] and Nd^{3+},Cr^{3+}:GSGG we have analyzed over 400 zero-phonon transitions that establish the crystal-field splitting of Nd^{3+} and Gd^{3+} energy levels in the lattice. The vibronic spectrum of Cr^{3+} in C_{3i} sites has been analyzed to determine the approximate location of the electronic levels of Cr^{3+}. A Hamiltonian consisting of Coulombic, spin-orbit, and crystal-field terms corresponding to the symmetry appropriate to each ion was diagonalized to obtain theoretical energy levels. The rms deviation between calculated and observed levels is 1.7 cm^{-1} for Nd^{3+} (45 levels), 4 cm^{-1} for Gd^{3+} (14 levels), and 87.7 cm^{-1} for Cr^{3+} (35 levels). The lattice-sum calculations for both Nd^{3+} and Cr^{3+} are in reasonable agreement with the empirical parameters obtained from fitting the observed energy levels. The C_{3i} point-group symmetry of the lattice must be used to interpret the energy levels of Cr^{3+} in GSGG.

ACKNOWLEDGMENTS

One of us (J.B.G.) wishes to thank the American Society for Engineering Education for their support while spectra were taken at the Naval Weapons Center, China Lake, CA. Two others (C.A.M. and G.A.T.) wish to thank Dr. R.P. Leavitt for considerable assistance with the computer programming of the d^N configuration. We also wish to thank Dr. M. Nadler, Chemistry Division, Naval Weapons Center, for recording the FTIR spectra.

[1]A. A. Kaminskii, Kh. S. Bagdasarov, G. A. Bogomolova, M. M. Gritsenko, A. M. Kevorkov, and S. E. Sarkisov, Phys. Status Solidi A **34**, K109 (1976).

[2]B. Struve, G. Huber, V. V. Laptev, I. A. Shcherbakov, and E. V. Zharikov, Appl. Phys. **B28**, 235 (1982); **30**, 117 (1983).

[3]A. Beimowski, G. Huber, D. Pruss, V. V. Laptev, I. A. Shcherbakov, and E. V. Zharikov, Appl. Phys. **B28**, 234 (1982).

[4]D. Pruss, G. Huber, and A. Beimowski, Appl. Phys. **B28**, 355 (1982).

[5]E. V. Zharikov, V. V. Laptev, E. I. Sidorova, Yu. P. Timofeev, and I. A. Shcherbakov, Kvant. Elektron. **9**, 1740 (1982) [Sov. J. Quantum Electron. **12**, 1124 (1982)].

[6]E. V. Zharikov, N. N. Ill'ichev, V. V. Laptev, A. A. Malyutin, V. G. Ostroumov, P. P. Pashinin, and I. A. Shcherbakov, Kvant. Elektron. (Moscow) **9**, 568 (1982) [Sov. J. Quantum Electron. **12**, 338 (1982)].

[7]E. V. Zharikov, N. N. Ill'ichev, S. P. Kalitin, V. V. Laptev, A. A. Malyutin, V. V. Osiko, V. G. Ostroumov, P. P. Pashinin, A. M. Prokhorov, V. A. Smirnov, A. F. Umyskov, and I. A. Shcherbakov, Kvant. Elektron. (Moscow) **10**, 1916 (1983) [Sov. J. Quantum Electron. **13**, 1274 (1983)].

[8]M. I. Demchouk, A. K. Gilev, A. M. Zabaznov, V. P. Mikhailov, A. A. Stavrov, and A. P. Shkadarevich, Opt. Commun. **55**, 207 (1985).

[9]E. Reed, IEEE J. Quantum Electron. **QE-21**, 1625 (1985).

[10]M. Sekita, Y. Miyazawa, and S. Kimura, J. Appl. Phys. **58**, 3658 (1985).

[11]W. F. Krupke, M. D. Shinn, J. E. Marion, J. A. Caird, and S. E. Stokowskii, J. Opt. Soc. Am. **B3**, 102 (1986).

[12]C. A. Morrison, U.S. Army Harry Diamond Laboratories Report No. HDL-TR-2040, 1984 (unpublished).

[13]J. B. Gruber, M. E. Hills, M. P. Nadler, M. R. Kokta, and C. A. Morrison, Bull. Am. Phys. Soc. **31**, 243 (1986).

[14]C. A. Morrison and R. P. Leavitt, in *Handbook on the Physics and Chemistry of Rare Earths V*, edited by K. A. Gschneidner, Jr. and L. Eyring (Pergamon, New York, 1982).

[15]R. Reisfeld and C. K. Jorgensen, *Lasers and Excited States of Rare Earths* (Springer, New York, 1977).

[16]A. A. Kaminskii, *Laser Crystals* (Springer, New York, 1981).

[17]B. Struve and G. Huber, Appl. Phys. B **36**, 195 (1985).

[18]S. Sugano and Y. Tanabe, J. Phys. Soc. Jpn. **13**, 880 (1958).

[19]S. Sugano and I. Tsujikawa, J. Phys. Soc. Jpn. **13**, 899 (1958).

[20]M. O. Henry, J. P. Larkin, and G. F. Imbusch, Proc. R. Irish Acad. **75**, 97 (1975).

[21]S. Geller, Z. Kristallogr. **125**, 1 (1967).

[22]G. I. Vetrogon, V. I. Danilenko, V. Ya. Kabanchenko, V. V. Osiko, A. M. Prokhorov, A. N. Terent'evskii, and M. I. Timoshechkin, Fiz. Tverd. Tela (Leningrad) **22**, 689 (1980) [Sov. Phys.—Solid State **22**, 1881 (1980)].

[23]C. A. Morrison, R. P. Leavitt, and M. D. Gildner, U.S. Army Harry Diamond Laboratories Report No. HDL-TR-2035, 1984 (unpublished).

[24]R. A. Satten, J. Chem. Phys. **27**, 286 (1957), and references therein.

[25]W. E. Bron, Phys. Rev. **140**, A2005 (1965), and references therein.

[26]J. B. Gruber, R. P. Leavitt, C. A. Morrison, and N. C. Chang, J. Chem. Phys. **82**, 5373 (1985) and references therein.

[27]W. T. Carnall, P. R. Fields, and K. Rajnak, J. Chem. Phys. **49**, 4412 (1968).

[28]C. A. Morrison, N. Karayianis, and D. E. Wortman, U.S. Army Harry Diamond Laboratories Report No. HDL-TR-1816, 1977 (unpublished).

[29]B. R. Judd, *Operator Techniques in Atomic Spectroscopy* (McGraw-Hill, New York, 1963), p. 162.

[30]P. H. M. Uylings, A. J. J. Raassen, and J. F. Wyart, J. Phys. B **17**, 4103 (1984).

[31]J. Sugar and C. Corliss, J. Phys. Chem. Ref. Data **6**, 137 (1977).

[32]C. W. Nielson and G. F. Koster, *Spectroscopic Coefficients for the p^n, d^n, and f^n Configurations* (MIT, Cambridge, MA, 1963).

[33]G. F. Koster, J. O. Dimmock, R. G. Wheeler, and H. Statz, *Properties of the Thirty-Two Point Groups* (MIT, Cambridge, MA, 1963).

[34]Y. Tanabe and S. Sugano, J. Phys. Soc. Jpn. **11**, 864 (1956).

[35]D. T. Sviridov, R. K. Sviridova, N. I. Kulik, and V. B. Glasko, J. Appl. Spectrosc. **30**, 334 (1979).

[36]R. P. Leavitt, J. Chem. Phys. **7**, 1661 (1982).

[37]S. Fraga, L. M. S. Saxena, and J. Karwowski, *Physical Science Data: 5. Handbook of Atomic Data* (Elsevier, Amsterdam, 1976).

[38]C. O. Brandle and R. L. Barns, J. Cryst. Growth **20**, 1 (1979).

[39]F. Euler and J. A. Bruce, Acta Cryst. **19**, 971 (1965).